Structure of Isolated 1,4-Butanediol: Combination of MP2 Calculations, NBO Analysis, and Matrix-Isolation Infrared Spectroscopy

A. J. Lopes Jesus,*,‡ Mário T. S. Rosado,† Igor Reva,† Rui Fausto,† M. Ermelinda S. Eusébio,† and J. S. Redinha†

Department of Chemistry, University of Coimbra, 3004-535, Coimbra, Portugal, and Faculty of Pharmacy, University of Coimbra, 3004-295, Coimbra, Portugal

Received: December 10, 2007; Revised Manuscript Received: February 28, 2008

Theoretical calculations at the MP2 level, NBO and AIM analysis, and matrix-isolation infrared spectroscopy have been used to investigate the structure of the isolated molecule of 1,4-butanediol (1,4-BDO). Sixty-five structures were found to be minima on the potential energy surface, and the three most stable forms are characterized by a folded backbone conformation leading to the formation of an intramolecular H-bond. To better characterize the intramolecular interactions and particularly the hydrogen bonds, natural bond orbital analysis (NBO) was performed for the four most stable conformers, and was further complemented with an atoms-in-molecules (AIM) topological analysis. Infrared spectra of 1,4-BDO isolated in low-temperature argon and xenon matrixes show a good agreement with a population-weighted mean theoretical spectrum, and the spectral features of the conformers expected to be trapped in the matrixes were observed experimentally. Annealing the xenon matrix from 20 to 60 K resulted in significant spectral changes, which were interpreted based on the barriers to intramolecular rotation. An estimation of the intramolecular hydrogen bond energy was carried out following three different methodologies.

Downloaded by PORTUGAL CONSORTIA MASTER on July 6, 2009
Published on April 30, 2008 on http://pubs.acs.org | doi: 10.1021/jp7116196

1. Introduction

Butanediols form a group of compounds that have numerous applications in the biochemical field, namely in cryobiology,[1–4] and as protein-stabilizing agents.[5,6] In addition, they represent an important molecular fragment present in many macromolecules of biological interest. In industry, they are also used as intermediates in the production of polyurethanes and as humectants in pet foods, tobacco, and cosmetics formulations.[7]

Following the investigation performed by our research group on the structure of butanediols,[8–12] the present paper is dedicated to 1,4-butanediol (1,4-BDO). A few available theoretical studies performed on this molecule, reporting only the structures and energies of a reduced number of conformations, have been published.[13–15] Experimentally, infrared spectroscopy studies in dilute solutions of inert solvents at room temperature have been used to assert the existence of intramolecular hydrogen bonds.[9,16–19]

A more extensive study on the structure of isolated 1,4-BDO was performed by Trætteberg et al.[20] These authors used gas-phase electron diffraction combined with molecular mechanics calculations and concluded that the hydrogen-bonded conformers are presented in a significant amount in the gas phase (40 % at 144 °C and 33 % at 260 °C). A value of about 10−11 kJ mol^{-1} has been obtained as a rough estimate of the average intramolecular hydrogen bond energy. This value is close to the one reported by Shagidullin et al.[19] (ca. 15 kJ mol^{-1}) derived from the combination of infrared studies in CCl_4 solutions and molecular mechanics calculations, but well below than that estimated by Mandado et al. (ca. 24 kJ mol^{-1}) based on the quantum theory of atoms in molecules (QTAIM).[13]

The research program followed in the present paper consists of an exhaustive conformational analysis of 1,4-BDO using high-level theoretical methods and the study of its molecular electronic structure by natural bond orbital (NBO) analysis. The intramolecular interactions in this molecule were further examined by means of an electron density topological study. The theoretical data are complemented by an infrared spectroscopy study of 1,4-BDO isolated in low-temperature argon and xenon matrixes. The combination of this technique with the theoretical data allowed the experimental identification and characterization of the conformers trapped in the matrix, as well as study of their possible interconversions.

2. Methods

2.1. Computational Methodology. The molecule of 1,4-BDO has five main torsion angles, with three of them characterizing the backbone structure (OCCC, CCCC, and CCCO) and the remaining related to the orientation of the two OH groups (HOCC). Letter codes will be used to describe the values of these dihedral angles. Hence, each conformation is identified by five letters (aBCDe) describing the orientation of the dihedrals $\varphi_1(H_1O_1C_1C_2)$, $\varphi_2(O_1C_1C_2C_3)$, $\varphi_3(C_1C_2C_3C_4)$, $\varphi_4(C_2C_3C_4O_4)$, and $\varphi_5(C_3C_4O_4H_4)$, respectively (see Figure 1 for the atom numbering scheme).

Assuming three possible minima per torsion, i.e., trans (180° ± 30°), +gauche (60° ± 30°), and −gauche (−60° ± 30°), abbreviated by "t" or "T", "g" or "G" and "g′" or "G′" (capital letters refer to the backbone structure while the lower case ones refer to the OH orientations), respectively, the total number of possible conformations is $3^5 = 243$. However, symmetry considerations reduce this number to 70 unique conformations. All of these 70 initial structures were fully optimized at the MP2 level of theory[21–23] using the 6-311++G(d,p) triple-ζ split-valence basis set. A tight optimization criterion was used in all calculations. Additionally, harmonic vibrational frequencies were

* Corresponding author: E-mail: ajorge@qui.uc.pt.
† Department of Chemistry.
‡ Faculty of Pharmacy.

10.1021/jp7116196 CCC: $40.75 © 2008 American Chemical Society
Published on Web 04/30/2008

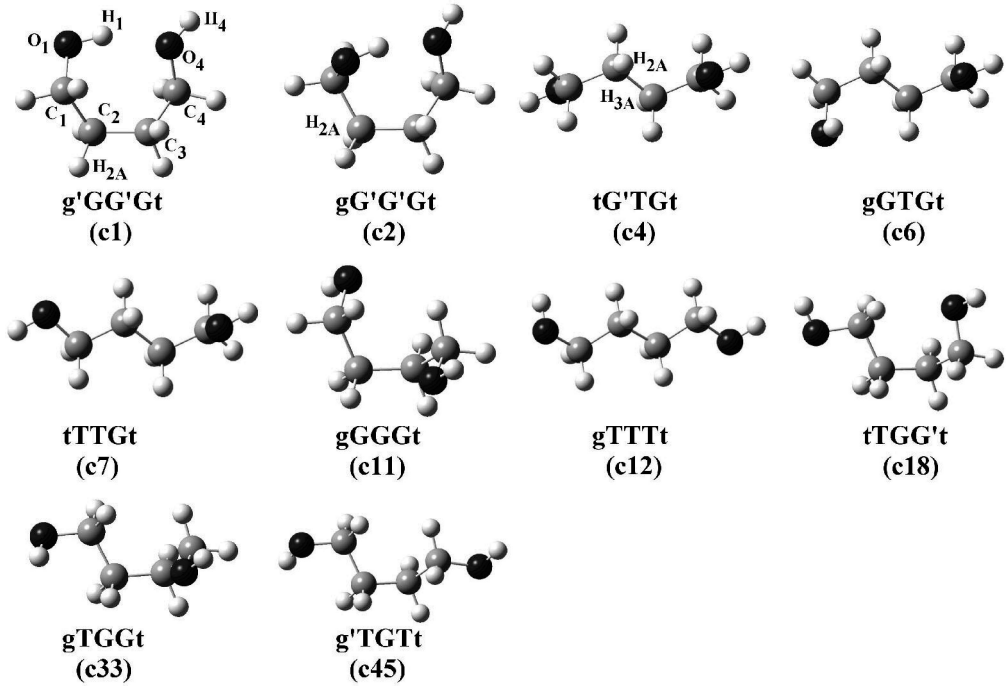

Figure 1. MP2/6-311++G(d,p) optimized geometries of the most populated conformers of each of the backbone families of 1,4-butanediol in the gas phase at 298.15 K. The atom numbering scheme is given in c1. Some hydrogen atoms connected to carbon atoms C_2 and C_3 are labeled as H_{2A} and H_{3A}, respectively.

Downloaded by PORTUGAL CONSORTIA MASTER on July 6, 2009
Published on April 30, 2008 on http://pubs.acs.org | doi: 10.1021/jp7116196

calculated to characterize the nature of each stationary point. The determination of the Hessian matrix also enabled calculation of the thermochemical quantities for the conformers at 298.15 K.

Barriers to intramolecular rotation were calculated for some selected pairs of conformers. Transition state geometries were obtained using the synchronous transit-guided quasi-Newton method (STQN) with the quadratic synchronous transit (QST) approach,[24] in its QST2 variety. All transition states were characterized as first-order saddle points by the presence of one imaginary frequency, as revealed by analysis of the corresponding Hessian matrices. All calculations mentioned above were performed with the Gaussian 03 program package.[25]

To better understand the specific nature of the intramolecular interactions involved in the 1,4-butanediol structure, a set of the most important conformers was selected to characterize their electronic structure by natural bond orbital (NBO) analysis. This was carried out using the NBO 5.G program[26] linked to the GAMESS software package,[27] version 22-Feb-2006 (R5). All NBO calculations were also performed at the MP2/6-311++G(d,p) level of theory.

The results of the NBO analysis were complemented with a topological analysis of electron density based on the theory of atoms in molecules (AIM).[28] The wave function was calculated from the MP2 optimized geometries using the Gaussian 03 program, while the bond critical points (BCPs) were located and characterized using the Extreme program[29] included in the AIMPAC software package.[30]

2.2. Experimental Procedures. Commercial 1,4-BDO (Aldrich, >99%) was used in the present work. The purity of the compound was checked by GLC using polar (DB-Wax polyethylene glycol) and nonpolar (OV-1 polydimethylsiloxane) columns. The values obtained were in the range of 99.1−99.8%. Since the compound is hygroscopic, the samples for the matrix-isolation infrared spectroscopy experiments were loaded into an effusive Knudsen cell inside a glovebox under a dry nitrogen atmosphere. The Knudsen cell was connected to the cryostat through an SS-4BMRG (NUPRO) needle valve. The valve was kept at 298 K, and this temperature defined the equilibrium ratio of butanediol conformers in the vapor before deposition. Before the experiment, the cell was connected to the vacuum system of the cryostat and the compound was additionally purified from dissolved gases using pumping.

The deposition rate of the compound was chosen low enough to ensure that the species trapped in matrixes were mostly monomers. A CsI window was used as optical substrate for the matrixes. Its temperature was stabilized at 10 and 20 K for argon and xenon matrixes, respectively, and measured directly at the sample holder by a silicon diode sensor connected to a digital controller (Scientific Instruments, Model 9650-1), with an accuracy of 0.1 K.

A glass vacuum system and standard manometric procedures were applied to deposit matrix gases (argon N60 and xenon N45, supplied by Air Liquide), which were used without further purification. The low-temperature equipment was based on a closed-cycle helium refrigerator (APD Cryogenics) with a DE-202A expander. Infrared spectra were registered with resolution of 0.5 cm^{-1}, in the range 4000−400 cm^{-1}, using a Mattson (Infinity 60AR Series) Fourier transform infrared spectrometer equipped with a deuterated triglycine sulfate (DTGS) detector and a KBr beamsplitter. Modifications of the sample compartment of the spectrometer were made in order to couple it with the cryostat head and allow purging of the instrument by a stream of dry nitrogen to remove carbon dioxide and water vapors.

3. Results and Discussion

3.1. Conformational Analysis. From the 70 predicted unique conformations, four structures converged to other minima (tGG′Gg → g′GG′Gg, gG′G′Gg → gG′G′Gt, g′G′G′Gg → g′G′G′Gg′, and gG′G′Gg′ → g′G′G′Gg′) and one, tGG′Gt, was

found to be a first-order transition state. The remaining 65 initial conformations were found to be minima on the potential energy surface.

The electronic energy values obtained after geometry optimization were corrected with the zero-point vibrational energy, giving the total energy at 0 K (E_0). Translational, rotational, and vibrational thermal energies were added to this value in order to obtain the enthalpy at 298.15 K. From this quantity and that calculated for the entropy, the Gibbs energy was determined using standard thermodynamics. The relative weight of each conformer in the gas-phase equilibrium was obtained from the Boltzmann distribution based on the Gibbs energy values at 298.15 K. The dihedral angles defining the structure of the conformers, as well as their total energies at 0 K, enthalpies, Gibbs energies, and equilibrium populations at 298.15 K are given in Table 1 in ascending Gibbs energy order. The optimized geometries of some conformers of 1,4-BDO are shown in Figure 1.

The data displayed in Table 1 allow characterization of the conformers, from both the geometric and thermodynamic points of view. Through the values of dihedrals, bond angles, and distances, one can get an insight into their molecular structures. The distortion from the natural values of gauche and trans dihedrals was investigated by cluster analysis, using the *K*-means method. All 1125 dihedral values corresponding to the internal rotations of all 225 conformers, including degenerated forms, were sampled. For each orientation, the number of clusters (K) was chosen such that no significant decrease in the variance within each cluster was observed by increasing K. Ignoring four trans outliers, the ideal number of clusters for each orientation is five. Following this procedure, it was found that the preferred value for the gauche orientations was $\pm 62.7 \pm 1.7°$ (171 counts out of 346), whereas for the trans orientation this value was $180.0 \pm 1.6°$ (123 cases out of 433). Figure 2 shows the distribution of the dihedral angle clusters. The gauche clusters are spread over a greater range and have larger standard deviations. However, there is a significant preference for the 62.7° value, by large the most populated. The trans clusters are limited to a narrower and more symmetrical interval, centered around 180°. This reflects the greater strain caused by the folded backbone arrangements of the gauche dihedrals. As can be seen in Table 1, all the conformers with a relative population higher than 1% comprise about 83% of the total conformational composition at 298.15 K. The forms c1, c2, c3, c13, and c16 are those with dihedral angles exhibiting a larger deviation from the most preferred values. As all of them are characterized by a folded backbone arrangement, it can be inferred that atypical dihedral angles in these conformers are caused by the minimization of steric repulsions and/or by the establishment of specific interactions between the two OH groups, namely intramolecular hydrogen bonds.

The usual geometric parameters related with H-bonding are the $H\cdots O_D$ and O_A-H distances, as well as the $O_A-H\cdots O_D$ angle, where O_A and O_D are the electron acceptor and donor oxygen atoms, respectively. The cutoff limits generally accepted for the establishment of a hydrogen bond are $H\cdots O_D < 3.0-3.2$ Å and $O_A-H\cdots O_D > 110°$.[31,32] According to these geometric criteria, hydrogen bonding is present in c1, c2, c3, c13, c16, and c39. The values of the geometric hydrogen bond parameters obtained for these conformers are given in Table 2.

It is thus clear that the distortion of some of the dihedrals is related to the establishment of intramolecular hydrogen bonds. In the case of c1, c2, and c3, the destabilization of their structures resulting from the distortion of φ_2 and φ_4 (c1 and c3) and φ_1 and φ_4 (c2) is compensated by the stabilization due to the intramolecular H-bond, making them the three most stable conformers. Concerning c13 and c16, in spite of the formation of an H-bond, the high distortion of φ_2 and φ_5 (c13) and φ_1, φ_4, and φ_5 (c16) (see Table 1) destabilizes these structures.

For all conformers presented in Table 1, the calculated ΔE and ΔG values fall within a range of about 28 and 30 kJ mol^{-1}, respectively, above the most stable conformer c1. All dihedral angles in this conformer are gauche, except φ_5, which assumes a trans orientation. Conformer c2 also presents a folded structure but differs from c1 by φ_1 and φ_2, which have g and G′ orientation, respectively (instead of g′ and G). This conformer has an enthalpy only 0.5 kJ mol^{-1} above that of c1. Since the entropy of c2 is lower than that of c1, its relative Gibbs energy increases by 1.3 kJ mol^{-1}. Conformer c3 is very similar to c1, with the only difference lying in the orientation of φ_5, which is gauche in c3 and trans in c1. This conformational change corresponds to ΔH and ΔG increases of 1.2 and 1.9 kJ mol^{-1}, respectively. Conformer c4 exhibits a rather different structure type. The trans orientation around φ_3 results in a more distended backbone, accompanied by a pronounced enthalpy increase (6.6 kJ mol^{-1}). The entropic compensation ($T\Delta S = 3.3$ kJ mol^{-1}) attenuates the ΔG increase (3.3 kJ mol^{-1}). The structure of c5 is similar to that of c4. However, the variation of φ_5 from the preferred trans to gauche orientation yields an enthalpy increase of 1.6 kJ mol^{-1}, which is greatly compensated by the entropy, resulting in a ΔG increase of only 0.7 kJ mol^{-1}.

From c5 onward, irregular and sometimes accentuated variations of ΔH between consecutive conformers are almost compensated by the entropy variations. This behavior is particularly noticeable for the H-bonded conformers (see Table 1). As a result, with only a few exceptions, small and regular variations of ΔG are found.

3.2. NBO Analysis. NBO analysis provides an electronic structure description akin to the classic Lewis bonding theory.[33–36] Filled NBOs, empty bond NBOs, and non-Lewis extra valence Rydberg orbitals, as well as their interactions, are considered in this analysis. The interaction between filled and empty NBOs corresponds to the electron delocalization from the former to the latter orbital and can be described as a hyperconjugative electron transfer process from the donor (filled) to the acceptor (vacant) orbital. The energy lowering of the donor orbital $\Phi_i^{(0)}$ and the acceptor orbital $\Phi_{j^*}^{(0)}$ ($E_{i,j^*}^{(2)}$), calculated as a second-order perturbation, is given by[33–35]

$$E_{i,j^*}^{(2)} = -n_i^{(0)} \frac{\langle \Phi_i^{(0)} | \hat{F} | \Phi_{j^*}^{(0)} \rangle^2}{\varepsilon_{j^*}^{(0)} - \varepsilon_i^{(0)}} = -n_i^{(0)} \frac{K^2 S_{i,j^*}}{\varepsilon_{j^*}^{(0)} - \varepsilon_i^{(0)}} \quad (1)$$

where $n_i^{(0)}$ is the i orbital occupancy, while ϵ_{j^*} and ϵ_i are the energies of the antibonding and bonding orbitals, respectively. The numerator of the second member is the Fock matrix element involving the two-center Φ_i orbital. The Fock matrix element is approximately proportional to the pre-NBO overlap integral (S_{i,j^*}), which can be also used to evaluate the donor−acceptor NBO interactions. As the orbitals i and j approach each other, repulsion energy arises due to the Pauli exclusion principle and is given by[37]

$$E_{\text{total}}^{(\text{st})} = \sum_i \left(F_{i,i}^{(\text{LNMO})} - F_{i,i}^{(\text{PLNMO})} \right) \quad (2)$$

$F_{i,i}^{(\text{LNMO})}$ is the energy of the localized natural molecular orbital, and $F_{i,i}^{(\text{PLNMO})}$ is the energy of the Pauli-violating preorthogonal LNMO (PLNMO). The steric interaction of

Downloaded by PORTUGAL CONSORTIA MASTER on July 6, 2009
Published on April 30, 2008 on http://pubs.acs.org | doi: 10.1021/jp7116196

TABLE 1: Dihedral Angles, Symmetry Point Groups, Relative Energies, and Equilibrium Populations at 298.15 K of the Conformers of 1,4-Butanediol Calculated at the MP2/6-311++G(d,p) Level of Theory[a]

		dihedral angles/deg[b]										
conf.	label	φ_1	φ_2	φ_3	φ_4	φ_5	sym[c]	ΔE_0/kJ mol^{-1}	ΔH/kJ mol^{-1}	$T\Delta S$/kJ mol^{-1}	ΔG/kJ mol^{-1} [d]	pop.[e]
c1	g′GG′Gt	−63.1	75.8	−71.6	73.7	174.6	C_1	0.00	0.00	0.00	0.00	20.41
c2	gG′G′Gt	77.5	−53.1	−52.4	77.5	−176.5	C_1	0.45	0.52	−0.80	1.32	12.01
c3	g′GG′Gg	−67.2	76.6	−65.7	72.0	67.6	C_1	1.39	1.25	−0.67	1.92	9.40
c4	tG′TGt	−179.9	−61.2	189.0	61.2	179.9	C_i	4.68	6.65	3.33	3.32	5.34
c5	tG′TGg	−177.8	−60.0	−175.9	62.0	62.5	C_1	6.68	8.28	4.24	4.04	3.99
c6	gGTGt	57.5	61.8	−177.1	61.9	177.9	C_1	7.03	8.64	4.43	4.21	3.74
c7	tTTGt	−173.9	−177.5	−179.8	63.1	−178.1	C_1	8.49	11.00	6.62	4.38	3.48
c8	g′TTGt	−56.3	−177.6	−179.6	61.9	179.7	C_1	7.80	9.64	4.84	4.80	2.94
c9	tG′TGg′	179.8	−62.7	175.4	62.9	−66.7	C_1	8.04	9.98	5.13	4.85	2.89
c10	tTTGg′	179.9	178.9	176.0	64.2	−64.7	C_1	9.46	11.93	6.65	5.28	2.43
c11	gGGGt	63.1	54.6	54.8	54.2	177.8	C_1	6.94	7.92	2.43	5.50	2.22
c12	gTTTt	58.4	177.3	−179.9	−179.5	−177.5	C_1	10.00	12.60	6.81	5.79	1.97
c13	tG′G′Gg	−171.0	−48.7	−57.2	67.7	19.8	C_1	6.44	7.07	1.15	5.92	1.88
c14	gTTGt	55.1	177.3	177.5	61.0	178.9	C_1	9.12	11.03	5.03	6.00	1.81
c15	tTTGg	−179.8	−179.0	−177.0	62.4	62.2	C_1	10.41	12.72	6.42	6.31	1.60
c16	tG′G′Gg′	−167.8	−51.6	−50.1	80.2	−14.7	C_1	7.03	7.38	0.92	6.46	1.51
c17	g′GTGt	−58.5	67.2	176.5	62.2	179.7	C_1	9.98	11.79	5.03	6.76	1.34
c18	tTGG′t	169.2	169.9	68.3	−70.2	−176.7	C_1	10.50	12.47	5.44	7.03	1.20
c19	tG′G′Gt	162.9	−65.4	−84.0	63.2	179.9	C_1	10.46	12.19	4.86	7.34	1.06
c20	tTTTt	180.0	180.0	180.0	180.0	180.0	C_{2h}	8.39	11.94	4.53	7.41	1.03
c21	g′TTGg	−55.6	−176.4	−175.4	62.7	65.0	C_1	10.21	11.78	4.29	7.49	1.00
c22	g′G′TGg	−63.2	−61.0	180.0	61.0	63.2	C_i	8.41	9.76	2.14	7.62	0.94
c23	gG′TGg	65.3	−63.0	−172.9	62.5	64.7	C_1	10.42	11.99	4.23	7.76	0.89
c24	gTTGg	56.1	177.0	−179.8	60.8	62.4	C_1	10.77	12.38	4.47	7.92	0.84
c25	g′TTGg′	−59.8	−178.4	175.0	62.9	−68.9	C_1	11.08	12.89	4.80	8.10	0.78
c26	tGGGt	176.2	54.8	55.1	54.8	176.2	C_2	5.94	6.98	−1.16	8.14	0.77
c27	g′TGG′t	−177.6	−70.1	70.1	176.4	−57.2	C_1	11.76	13.42	5.09	8.33	0.71
c28	g′GTGg	−66.7	64.6	178.1	60.8	61.5	C_1	11.37	13.01	4.67	8.34	0.71
c29	gTTGg′	59.5	176.6	176.3	64.9	−63.1	C_1	11.33	13.05	4.58	8.47	0.67
c30	gTGG′t	63.0	174.6	84.0	−62.1	−177.7	C_1	12.34	14.08	5.56	8.51	0.66
c31	g′GGGt	−63.7	61.5	57.1	55.0	176.3	C_1	10.71	12.12	3.59	8.54	0.65
c32	tGTGt	178.3	60.4	174.2	60.4	178.3	C_2	8.05	9.97	1.43	8.55	0.65
c33	gTGGt	57.2	173.2	58.7	53.8	176.2	C_1	10.49	11.72	3.18	8.55	0.65
c34	gTGGg	59.7	172.6	61.2	54.6	64.7	C_1	12.11	13.49	4.13	9.36	0.47
c35	gG′TGg′	68.0	−64.2	180.0	64.2	−68.0	C_i	11.01	12.90	3.47	9.43	0.45
c36	gGTGg	62.4	63.9	−169.1	63.9	62.4	C_2	8.31	9.47	0.03	9.44	0.45
c37	g′TGGt	−53.5	176.7	59.7	55.4	178.4	C_1	11.60	12.92	3.47	9.45	0.45
c38	tTGGt	167.4	170.6	57.9	54.6	175.7	C_1	11.68	13.24	3.78	9.45	0.45
c39	g′G′G′Gg′	−59.2	−50.2	−47.2	85.3	−31.1	C_1	8.82	8.76	−0.97	9.72	0.40
c40	g′GG′Gg′	−69.6	65.4	−96.0	65.4	−69.6	C_2	9.24	10.47	0.74	9.73	0.40
c41	tTGGg	166.7	169.9	57.4	53.8	61.7	C_1	12.28	13.82	3.96	9.86	0.38
c42	g′GGGg	−72.6	59.5	57.9	55.0	63.5	C_1	12.39	13.87	3.99	9.88	0.38
c43	g′TTTg	−58.6	−177.3	180.0	177.3	58.6	C_i	11.10	12.96	3.05	9.91	0.38
c44	tTGG′g′	166.8	171.1	63.5	−71.5	−67.5	C_1	12.29	14.04	4.11	9.92	0.37
c45	g′TGTt	−56.2	177.1	62.7	171.2	172.7	C_1	13.11	15.06	4.86	10.20	0.33
c46	tTGGg′	178.1	174.9	62.3	60.4	−70.8	C_1	13.50	15.44	5.23	10.21	0.33
c47	gGGGg	64.8	54.0	55.4	54.0	64.8	C_2	8.93	10.01	−0.35	10.35	0.31
c48	g′TGGg	−55.3	175.7	60.4	55.0	62.9	C_1	13.50	14.85	3.92	10.93	0.25
c49	gTGTt	57.2	171.3	62.1	170.8	171.6	C_1	13.92	15.87	4.82	11.05	0.24
c50	gTGG′g′	63.1	170.4	67.8	−69.2	−66.6	C_1	14.03	15.68	4.43	11.26	0.22
c51	g′TGGg′	−56.2	179.9	61.9	60.1	−68.0	C_1	14.05	15.59	4.26	11.33	0.21
c52	g′G′G′Gt	−62.1	−64.3	−89.9	59.5	−179.2	C_1	13.10	14.27	2.89	11.38	0.21
c53	gTTTg	58.1	176.9	178.9	176.9	58.1	C_2	11.41	13.27	1.31	11.96	0.16
c54	g′TGG′g′	−56.4	176.7	65.4	−71.0	−67.1	C_1	14.15	15.60	3.62	11.98	0.16
c55	g′GTGg′	−62.2	66.6	176.4	66.6	−62.2	C_2	11.89	13.53	1.43	12.10	0.15
c56	tTGTt	175.2	171.9	62.2	171.9	175.2	C_2	12.58	15.14	2.96	12.19	0.15
c57	g′TGTg	−56.1	177.0	63.7	171.2	59.1	C_1	14.67	16.24	4.03	12.21	0.15
c58	gTGGg′	55.9	171.0	59.8	59.4	−70.7	C_1	15.54	17.24	4.64	12.60	0.13
c59	tTGG′g	177.9	167.5	65.8	−76.5	77.7	C_1	17.75	20.14	6.42	13.72	0.08
c60	g′GGGg′	−65.6	60.7	57.6	60.7	−65.6	C_2	14.65	16.37	1.20	15.17	0.04
c61	g′TGTg′	−56.9	177.1	63.4	177.1	−56.9	C_2	14.19	15.72	0.48	15.24	0.04
c62	g′TGG′g	−56.6	174.3	61.7	−81.0	75.4	C_1	18.84	20.77	5.12	15.65	0.04
c63	gTGTg	58.6	171.0	63.2	171.0	58.6	C_2	14.96	16.55	0.65	15.91	0.03
c64	gTGG′g	55.8	168.9	61.3	−81.4	70.2	C_1	19.57	21.18	4.01	17.17	0.02
c65	gGG′Gg	70.7	77.8	−45.4	77.8	70.7	C_2	27.71	28.94	−1.53	30.47	0.00

[a] All energies are relative to the most stable conformer (g′GG′Gt). The energies are listed with an exaggerated accuracy in order to enable a better gradation. Thermochemical quantities were calculated at 298.15 K. [b] $\varphi_1 = H_1O_1C_1C_2$; $\varphi_2 = O_1C_1C_2C_3$; $\varphi_3 = C_1C_2C_3C_4$; $\varphi_4 = C_2C_3C_4O_4$; $\varphi_5 = C_3C_4O_4H_4$. [c] Each symmetry point group is associated with the conformational degeneracy (g), given in parentheses: C_1 ($g = 4$), C_i ($g = 2$), C_2 ($g = 2$), and C_{2h} ($g = 1$). [d] Gibbs energies at 298.15 K account for the degeneracy by adding an $-RT \ln(g)$ term. [e] Boltzmann populations (%) were estimated on the basis of the relative Gibbs energies.

Downloaded by PORTUGAL CONSORTIA MASTER on July 6, 2009
Published on April 30, 2008 on http://pubs.acs.org | doi: 10.1021/jp7116196

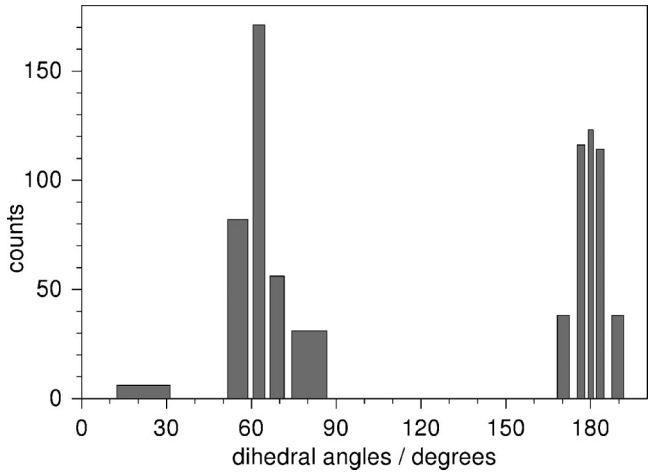

Figure 2. Distribution of *K*-means clusters of dihedral angles of the conformers of 1,4-BDO. The widths of the bars in the chart are proportional to the standard deviation of each cluster. The −gauche clusters are not shown as they are the mirror images of the +gauche.

TABLE 2: Geometric Parameters for the Conformers of 1,4-BDO Presenting Intramolecular Hydrogen Bonding

conformer	O_A−H/Å	$O_D\cdots$H/Å	O_A−H$\cdots O_D$/deg
c1	0.968	1.84	157
c2	0.966	2.02	142
c3	0.968	1.86	155
c13	0.964	2.15	136
c16	0.966	1.96	156
c39	0.966	1.94	160

individual orbital pairs i,j ($E_{i,j}^{(st)}$) is estimated by the following expression:[37]

$$E_{i,j}^{(st)} = \left(F_{i,i}^{(LNMO)} - F_{i,i}^{(PLNMO/2)}\right) + \left(F_{j,j}^{(LNMO)} - F_{j,j}^{(PLNMO/2)}\right) \quad (3)$$

Like the stabilizing orbital interactions, the pairwise orbital repulsion can be estimated by the respective overlap integral ($S_{i,j}$).

The NBO analysis was performed on the four lowest energy conformers. Altogether, they make up 47% of the conformational composition at 298.15 K and represent the two main types of structures presented by this molecule, i.e., bent (c1, c2, and c3) and distended conformers (c4).

The stabilizing and destabilizing energies of NBO interactions were considered down to 2 kJ mol^{-1}. A large diversity of energy values was found. The stronger donor character is shown by the p-type lone pair of the oxygen atoms. The hyperconjugative interactions between these orbitals and the antibonding orbitals of vicinal C−H or C−C bonds correspond to an $|E_{i,j^*}^{(2)}|$ as high as 46 kJ mol^{-1}. The interactions between the lone-pair orbitals and their vicinal C−C and C−H filled orbitals are the most energetic steric repulsions.

The NBO analysis gives information on which of $E_{i,j^*}^{(2)}$ and $E_{i,j}^{(st)}$ effects has a stronger influence on the energy of each conformer. From Table 3, one can see that for all studied conformers hyperconjugation overcomes the steric orbital repulsion. The energy difference between these quantities is more pronounced for c1 and c3, followed by c2 and then c4. Moreover, differences between conformers are more pronounced for hyperconjugation than for repulsion. The maximum differences between $E_{total}^{(st)}$ and $E_{total}^{(2)}$ among conformers are 11 and 79 kJ mol^{-1}, respectively.

TABLE 3: Total Stabilizing Donor−Acceptor Orbital Interaction, $E_{total}^{(2)}$, and Total Destabilizing Energy Orbital Repulsion, $E_{total}^{(st)}$ for the Four Most Stable Conformers of 1,4-BDO[a]

conformer	$E_{total}^{(2)}$/kJ mol^{-1}	$E_{total}^{(st)}$/kJ mol^{-1}
c1	−767.47	674.63
c2	−715.67	678.14
c3	−760.69	667.56
c4	−688.10	669.02

[a] $E_{total}^{(2)} = \sum E_{i,j^*}^{(2)}$ and $E_{total}^{(st)} = \sum E_{i,j}^{(st)}$.

Most stabilizing interactions take place between vicinal NBOs. Besides these, some interactions between remote filled and unfilled orbitals are also present. The last ones deserve particular attention owing to the influence they can play on the backbone conformation. Hyperconjugative and steric repulsive interactions between remote orbitals with absolute energy higher than 2 kJ mol^{-1} are listed in Table 4.

Conformers c1 and c3 exhibit a similar framework of orbital overlaps. The main stabilizing and destabilizing interactions involve the O_4 lone pairs as donors and the O_1H_1 antibond orbital, $\sigma^*(O_1H_1)$, as acceptor (Table 4), with the p-type oxygen lone pair (Lp_2O_4) being stronger donor than the sp-type lone pair (Lp_1O_4). Contrarily to the conformers referred above, the stronger donor orbital in c2 is Lp_1O_4. A representation of the interaction of the stronger donor lone pair of O_4 with the $\sigma^*(O_1H_1)$, and $\sigma(O_1H_1)$ orbitals is given in Figure 3 for c1 and c2.

On the grounds of the geometric parameters (Table 2), c1 and c3 exhibit an intramolecular H-bond. In c2, a weaker interaction of this type may also be present. An interpretation of the hydrogen bond is based on the following resonance hybrid:[33,38]

$$O_A{-}H \cdots O_D \leftrightarrow O_A^- \cdots HO_D^+$$

The dipole resulting from the charge transfer from O_D to O_A corresponds, in NBO terms, to the hyperconjugative interaction:

$$n(O_D) \rightarrow \sigma^*(O_AH)$$

According to the data of Table 4, one concludes that c1 and c3 are stabilized by an intramolecular H-bond between the two OH groups, in which both lone pairs of the donor oxygen atom are involved. The comparison of $E_{i,j^*}^{(2)}$ with $E_{i,j}^{(st)}$ and S_{i,j^*} with $S_{i,j}$ shows that this interaction contributes significantly to energy lowering in this structure. Regarding c2, the stabilization effect of the intramolecular H-bond is not so well evidenced as in the case of the c1 and c3 since $|E_{i,j^*}^{(2)}| < |E_{i,j}^{(st)}|$, despite $|S_{i,j^*}| > |S_{i,j}|$. In c4, interactions between the oxygen lone pairs and the OH groups are absent.

Hydrogen bonding manifests itself also in the hydrogen atomic charge of the acceptor group. The electron transfer from the O_4 lone pairs to the $\sigma^*(O_1H_1)$ orbital originates a repolarization of the acceptor, increasing the s character of the O_1 hybrid orbital. In turn, the increasing occupancy of $\sigma^*(O_1H_1)$ induces a repolarization of the $\sigma(O_1H_1)$ filled orbital, followed by a decrease of the H_1 electron population.[33] To illustrate these effects, let us consider the charge increase of the hydrogen atom involved in the H-bond in conformer c1. The NBO hybrid compositions of $\sigma(O_1H_1)$ and $\sigma(O_4H_4)$ are $0.8681(sp^{3.20})O_1 + 0.4963(s)H_1$ and $0.8581(sp^{3.71})O_4 + 0.5135(s)H_4$, respectively. Thus, hydrogen bonding increases the s character and the polarization coefficient of the O_1 hybrid orbital. The occupancy of $\sigma^*(O_1H_1)$ is 0.025*e*. With these results, the decrease of the

Downloaded by PORTUGAL CONSORTIA MASTER on July 6, 2009
Published on April 30, 2008 on http://pubs.acs.org | doi: 10.1021/jp7116196

TABLE 4: Summary of the NBO Analysis for the Remote Interactions Presented on the Four Most Stable Conformers of 1,4-BDO: Stabilization Energies ($E_{i,j^*}^{(2)}$), Steric Exchange Repulsion Energies ($E_{i,j}^{(st)}$), and Integral Overlaps ($|S_{i,j^*}|$ and $|S_{i,j}|$)[a]

	bond−antibond NBO interaction			pairwise steric NBO repulsion		
conformer	$\Phi_i \rightarrow \Phi_{j^*}$	$E_{i,j^*}^{(2)}$/kJ mol^{-1}	$\|S_{i,j^*}\|$	$\Phi_i \leftarrow \Phi_j$	$E_{i,j}^{(st)}$/kJ mol^{-1}	$\|S_{i,j}\|$
c1	$n(Lp_2O_4) \rightarrow \sigma^*(O_1H_1)$	−42.84	0.2254	$n(Lp_2O_4) \leftrightarrow \sigma(O_1H_1)$	34.27	0.1561
	$n(Lp_1O_4) \rightarrow \sigma^*(O_1H_1)$	−9.83	0.1038	$n(Lp_1O_4) \leftrightarrow \sigma(O_1H_1)$	5.77	0.0584
	$n(Lp_2O_1) \rightarrow \sigma^*(C_2H_{2A})$	−3.85	0.0914			
	$\sigma(O_4H_4) \rightarrow Ry^*(C_3)$	−4.94	0.0337			
c2	$n(Lp_1O_4) \rightarrow \sigma^*(O_1H_1)$	−13.97	0.1527	$n(Lp_1O_4) \leftrightarrow \sigma(O_1H_1)$	14.60	0.1000
	$n(Lp_2O_4) \rightarrow \sigma^*(O_1H_1)$	−3.10	0.0730	$n(Lp_2O_4) \leftrightarrow \sigma(O_1H_1)$	3.97	0.0595
	$n(Lp_2O_1) \rightarrow \sigma^*(C_2H_{2A})$	−4.69	0.1131	$n(Lp_2O_1) \leftrightarrow \sigma(C_2H_{2A})$	2.55	0.0272
	$\sigma(O_4H_4) \rightarrow Ry^*(C_3)$	−5.36	0.0429			
c3	$n(Lp_2O_4) \rightarrow \sigma^*(O_1H_1)$	−37.95	0.2432	$n(Lp_2O_4) \leftrightarrow \sigma(O_1H_1)$	32.30	0.1534
	$n(Lp_1O_4) \rightarrow \sigma^*(O_1H_1)$	−9.54	0.1029	$n(Lp_1O_4) \leftrightarrow \sigma(O_1H_1)$	5.19	0.0557
	$n(Lp_2O_1) \rightarrow \sigma^*(C_2H_{2A})$	−3.93	0.0940			
	$n(Lp_2O_4) \rightarrow \sigma^*(C_3H_{3A})$	−2.43	0.0996	$n(Lp_2O_4) \leftrightarrow \sigma(C_3H_{3A})$	2.43	0.0384
c4	$n(Lp_1O_4) \rightarrow \sigma^*(C_3H_{3A})$	−2.38	0.1054	$n(Lp_1O_4) \leftrightarrow \sigma(C_3H_{3A})$	3.35	0.0574
	$n(Lp_1O_1) \rightarrow \sigma^*(C_2H_{2A})$	−2.38	0.1054	$n(Lp_1O_1) \leftrightarrow \sigma(C_2H_{2A})$	3.35	0.0574
	$\sigma(O_4H_4) \rightarrow Ry^*(C_3)$	−4.90	0.0691			
	$\sigma(O_1H_1) \rightarrow Ry^*(C_2)$	−4.90	0.0691			

[a] Lp_2O_4 and Lp_1O_4 correspond to the p-type and sp-type oxygen lone pairs, respectively. Blank cells correspond to values lower than the threshold printing (2 kJ mol^{-1}).

Downloaded by PORTUGAL CONSORTIA MASTER on July 6, 2009
Published on April 30, 2008 on http://pubs.acs.org | doi: 10.1021/jp7116196

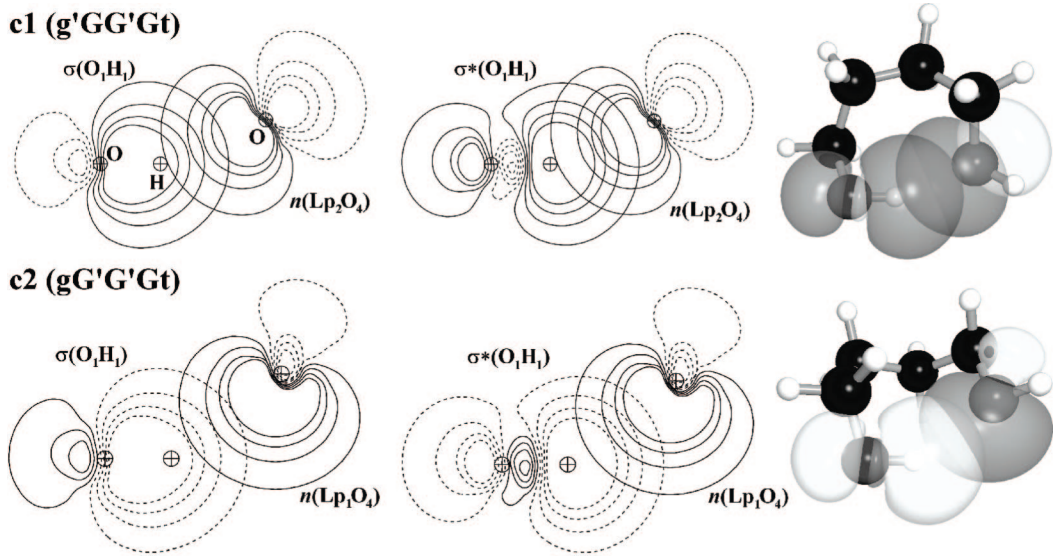

Figure 3. Contour plots of the of the preorthogonalized NBOs in c1 and c2 showing interaction of the stronger donor lone pair of O_4 with the $\sigma(O_1H_1)$ (left two contours), and $\sigma^*(O_1H_1)$ (middle two contours) orbitals and 3D representation of the n(O) → σ^*(OH) overlaps (right). In the four contours the centers of atoms involved in the H-bond are represented by circled crosses. These atoms are identified in the top left contour plot.

electron population at H_1 by repolarization, as consequence of the hydrogen bond, is $[(0.5135)^2 - (0.4963)^2](2e) = 0.034e$. The increase of electrons on the same atom due to the addition of $0.025e$ to $\sigma^*(O_1H_1)$ is $(0.8681)^2(0.025e) = 0.019e$. The estimate of the net electron reduction at H_1 is, therefore, $0.015e$. This is in agreement with the fact that the atomic charge on H_1 found in the natural population analysis is +0.491, whereas its natural atomic charge when it is free from a hydrogen bond is in the range of +0.456 to +0.469. In conformer c3, the atomic charge of H_1 is identical to that in c1 (+0.492), while in c2 the atomic charge on the same atom is +0.486.

Besides the intramolecular H-bonds, Table 4 also includes the energies of the remote interactions between the oxygen lone pairs and the $\sigma^*(C_2H_{2A})$ and $\sigma^*(C_3H_{3A})$ orbitals. These interactions are not discussed here as they contribute weakly to the structure stability.

3.3. AIM Topological Analysis. Atoms-in-molecules (AIM) electron density topological analysis, carried out for c1 and c2, revealed the existence of 15 bond critical points (BCPs) with a (3,−1) topology between the atoms connected by covalent bonds. Besides these, another (3,−1) BCP was located between the nonbonded H_1 and O_4 atoms.

Popelier proposed that the establishment of a hydrogen bond should be accompanied by four local topological properties of the electron density:[39,40] (1) existence of a (3,−1) BCP between the atoms involved in the interaction; (2) density at the BCP (ρ_{BCP}) in the range 0.002–0.040 au; (3) Laplacian of the density at the same point ($\nabla^2\rho_{BCP}$) is positive and in the range 0.015–0.15 au; and (4) existence of mutual penetration of hydrogen and the electron donor oxygen (O_D).

The values of ρ_{BCP} and $\nabla^2\rho_{BCP}$ obtained at the BCP between H_1 and O_4 were found to be, respectively, 0.032 60 and 0.117 9 au for c1 and 0.021 84 and 0.083 47 au for c2. These values are within the range meeting the referred criteria for the existence of a hydrogen bond. A further requirement for the existence of hydrogen bonding is interpenetration between the hydrogen and O_D. This implies that $r_H^0 > r_H$ and $r_D^0 > r_D$, where r_H and r_D are the distances from the nuclei of the H and O_D atoms to the BCP, while r_H^0 and r_D^0 are the corresponding nonbonded radii, usually given as the distance from the nucleus

Downloaded by PORTUGAL CONSORTIA MASTER on July 6, 2009
Published on April 30, 2008 on http://pubs.acs.org | doi: 10.1021/jp7116196

to the $\rho = 0.001$ au electron density contour.[28,39] A summary of the commonly adopted values for oxygen and hydrogen nonbonded radii is given elsewhere.[41] The value reported for oxygen is 1.68 Å, and those for hydrogen are 1.34 and 1.52 Å.[41] The values of r_H and r_D given in the output of the Extreme program are, respectively, 0.64 and 1.20 Å for c1, and 0.75 and 1.28 Å for c2. Hence, for both conformers this criterion is satisfied, thus indicating interpenetration between the two atoms.

The results of the AIM topological analysis confirm the existence of an intramolecular hydrogen bond in c1 as well as in c2, despite that for the latter conformer its presence is not so well evidenced by the NBO analysis. On the other hand, the comparison of ρ_{BCP} and $\nabla^2\rho_{BCP}$ for the two conformers also indicates that this interaction is stronger in c1 than in c2, which is consistent with the values of the geometric parameters reported in Table 2, with the results obtained from the NBO analysis, and with the relative stabilities of the two conformers shown in Table 1.

3.4. Interpretation of the Vibrational Spectra. In the interpretation of matrix-isolation experiments, it is generally accepted that the conformational distribution in the hot vapor (usually at room temperature) remains unaltered in the matrix. Therefore, the resulting infrared spectrum would contain spectral features of all conformers with a significant presence in the gas-phase equilibrium. However, this is only true when the conformers are separated by relatively high energy barriers (tens of kilojoules per mole). If the barriers are low enough (a few kilojoules per mole), intramolecular rotation can occur during the deposition of the compound in the matrix and, as a result, high energy conformers will relax to lower energy ones. This phenomenon is known as conformational cooling,[42–44] and can be expected to be relevant in such a flexible molecule as 1,4-butanediol. However, in order to investigate this possibility in detail, the barrier heights for conformational interconversion should be determined.

In our previous studies on the conformational features of the two diastereomers of 2,3-butanediol, it was found that rotations of the hydroxylic groups around the respective O−C bonds were associated with energy barriers lower than 5 kJ mol^{-1}. These barriers were easily overcome in the matrixes at a temperature as low as 10 K, resulting in the conversion of the higher energy conformers into their lower energy counterparts.[11] In that work, a concept of family of related conformers was introduced. A family included structures that shared the same heavy atom backbone and differed only in the orientation of the OH groups. The concept of grouping conformers was successfully applied in our subsequent matrix-isolation study on the structure of 1,2-butanediol.[12] In that study, an extensive calculation of barriers to intramolecular rotation of the hydroxylic groups showed that all these barriers did not exceed 5 kJ mol^{-1}. Moreover, it was shown that when the vapors of the compound were deposited into a cryogenic matrix, all conformers of the same family converted into its most stable member, while different families were preserved in the matrix after its deposition.[12] The latter finding was in agreement with the higher barriers separating structures with different heavy atom backbone conformation.

In order to interpret the vibrational spectra of 1,4-BDO, we applied the methodology which has proved to be successful for its positional isomers, 2,3-butanediol and 1,2-butanediol.[11,12] It was then assumed for 1,4-BDO that all structures differing by the orientation of the OH groups would relax to the most stable conformer of the respective family during deposition of the matrix at 10 K, due to the low energy barriers involved. This was checked by calculating the barriers for interconversions in c3/c1, c5/c4, c11/c26, c17/c6, and c7/c8 conformer pairs. At the MP2/6-311++G(d,p) level these barriers were found to be 1.8, 1.7, 2.2, 3.3, and 2.7 kJ mol^{-1}, respectively, thus supporting our assumption regarding the conformational relaxation within each family. Hence, only 10 conformers (one per family) would remain trapped in the matrix after deposition. These 10 conformers are listed in Table 5, and the optimized geometries of some of them are displayed in Figure 1.

TABLE 5: Calculated Boltzmann Populations at 298.15 K and the Most Stable Conformers in a Low-Temperature Matrix for All Backbone Families of 1,4-BDO

backbone family	family population at 298.15 K (%)[a]	lowest E_0 conformer within each family[b]	ΔE_0/kJ mol^{-1}
GG′G	30.21	c1	0.00
G′G′G	17.06	c2	0.45
TTG	15.55	c8	7.80
G′TG	14.51	c4	4.68
GTG	7.04	c6	7.03
GGG	4.38	c26	5.94
TTT	3.54	c20	8.39
TGG′	3.45	c18	10.50
TGG	3.32	c33	10.49
TGT	0.94	c56	12.58

[a] Values obtained by adding the Boltzmann populations of the conformers belonging to the same backbone family (see Table 1). [b] Conformer numbering according to Table 1; the conformers listed here are expected to be the most stable members of their respective families in a low-temperature matrix.

It is worth noticing that, at low temperature (10 K), the entropy and thermal energy are insignificant and the stability order of the conformers in the matrix is essentially due to the total energy at 0 K (E_0). Thus, it is expected that the conformer of each backbone type that remains in the matrix is the one with lower E_0. Its abundance in the matrix should correspond to the sum of the populations of all conformers belonging to the same backbone family, with the populations of individual conformers characteristic of the deposition temperature (298 K) (see Tables 1 and 5).

On the grounds of these assumptions, a theoretical spectrum of the conformational mixture expected to be trapped in the matrix after deposition was simulated, by adding the calculated spectra of conformers c1, c2, c8, c4, c6, c26, c20, c18, c33, and c56. The spectral intensities of each constituent were reduced by the net population of the corresponding family (see Table 5). The resulting population-weighted theoretical spectrum, together with the experimental spectrum of the compound isolated in an argon matrix at 10 K is displayed in Figure 4 (upper frame). This figure also includes the calculated frequencies and intensities of each component (lower frame). The close agreement between the experimental and simulated spectra confirms the validity of the assumptions here made regarding the conformational cooling and also the ability of the MP2/6-311++G(d,p) theoretical approach to predict accurately the conformational stability of these molecules, as well as their vibrational spectra.

The comparison between the experimental and the calculated spectra allows us also to verify the presence of some of the conformers in the matrix. For example, in the OH stretching region the bands at ca. 3585 cm^{-1} (multiplet) and ca. 3496 cm^{-1} (doublet) are assigned to c2 and c1, respectively. They correspond to the stretching vibration of the hydroxyl group involved in the intramolecular H-bond. The red shifts ($\Delta\upsilon$) of these two bands relative to the free OH stretching band ($\upsilon \approx$ 3662 cm^{-1}) are 166 and 77 cm^{-1} for c1 and c2, respectively.

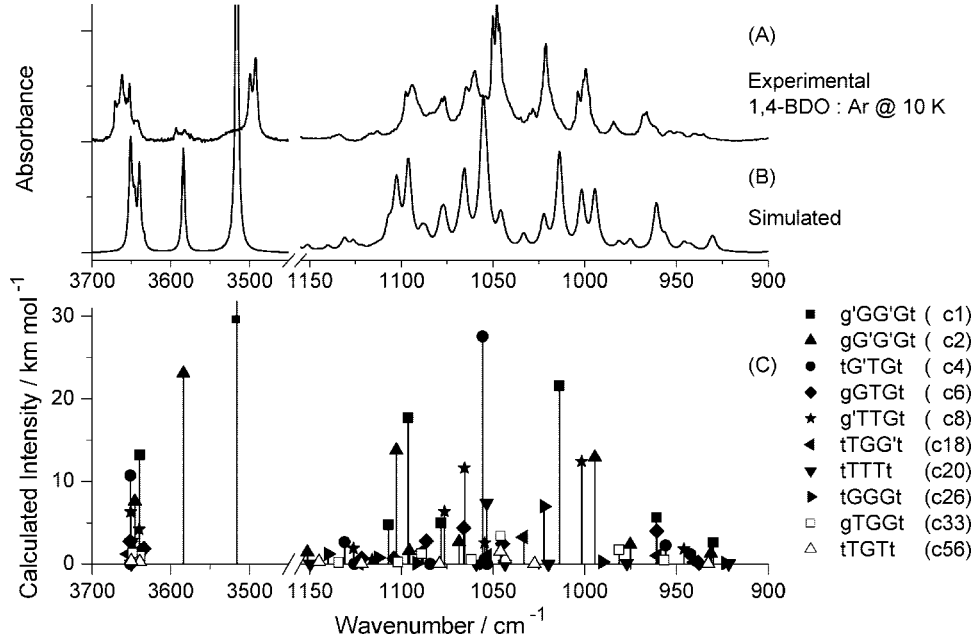

Figure 4. Experimental FTIR spectrum of 1,4-butanediol monomers isolated in an argon matrix at 10 K (A), simulated spectrum of a mixture of conformers (B), and theoretical spectra of the 10 most stable conformers (in matrix, one form per backbone family), calculated at the MP2/6-311++G(d,p) level (C). The calculated intensities in the individual spectra of conformers (C) were weighted by the population of the respective backbone family as described in Table 5. The simulated spectrum (B) was obtained using Lorentzian functions centered at the calculated frequencies and with a bandwidth at half-height equal to 4 cm^{-1}. The frequencies of the calculated spectra were scaled by two scaling factors: 0.937 (OH stretching region) and 0.963 (fingerprint region).

TABLE 6: Barriers for Intramolecular Rotation Calculated at the MP2/6-311++G(d,p) Level of Theory[a]

	family	GG′G	G′G′G	G′TG	GGG	GTG	TTG	TTT	TGG	TGG′	TGT
	conformer	c1	c2	c4	c26	c6	c8	c20	c33	c18	c56
family	conformer										
GG′G	c1	*									
G′G′G	c2	17.2	*								
G′TG	c4	d	11.6	*							
GGG	c26	21.2	25.4	d	*						
GTG	c6	5.3	d	22.0	10.3	*					
TTG	c8	d	d	13.3	d	15.0	*				
TTT	c20	t	t	d	t	d	14.1	*			
TGG	c33	d	11.7	d	13.7	d	8.1	d	*		
TGG′	c18	10.7	11.5	d	d	d	6.3	d	19.6	*	
TGT	c56	d	d	t	d	t	d	5.5	10.4	11.8	*

[a] Barrier values, including the zero-point vibrational energy, are in kJ mol^{-1} with respect to the less stable conformer in every pair. The reactant species are indicated in the second column, where they are ordered by ascending E_0. Only the barriers resulting in lowering of energy were studied (i.e. only half the table). d = double rotation, families (or their mirror images) that are separated by two barriers; t = triple rotation, families (or their mirror images) that are separated by three barriers.

Regarding the 1150−900 cm^{-1} region, the band at 1021 cm^{-1} is assigned to the most stable conformer, while that at 1048 cm^{-1} is due to c4. Some absorption bands have contributions of more than one conformer. For example, the band at ca. 1095 cm^{-1} is assigned to c1 and c2 and the same happens with the spectral feature at ca. 1000 cm^{-1}, which is due to c2 and c8. In addition, the band at ca. 1062 cm^{-1} is due to forms c8, c6, and c2. The presence of c26 is also confirmed by the weak absorption at 1029 cm^{-1}. The presence of the remaining five conformers in the matrix is more difficult to confirm experimentally because of their small abundance.

The energies required for intramolecular rotations about the C−C−C−C skeleton, i.e., barriers between the 10 forms remaining in the matrix, are shown in Table 6. Most of these interconversions involve energy barriers higher than 10 kJ mol^{-1}, and thus should occur only at temperatures higher than 10 K.[11,12,44] It is important to comment on the organization of Table 6. While conformational numbering is kept in the table according to the Gibbs free energies (see Table 1), the structures are ordered according to their total energies at 0 K:

$$c1 < c2 < c4 < c26 < c6 < c8 < c20 < c33 < c18 < c56$$

The reason for such ordering is related to the direction of the conformational interconversions expected in matrixes, as explained above.

In order to observe these interconversions experimentally, the argon matrix deposited at 10 K was subjected to annealing up to 33 K, which is close to the upper limit of thermal stability of solid argon. However, no significant spectral changes were observed. This behavior is in agreement with the relatively high energy barriers for the interconversions of the most populated forms in the matrix, which cannot be surpassed at relatively low temperatures. The occurrence of such transformations might only be possible in a matrix with stronger relaxant properties and with the possibility of annealing to higher temperatures. Therefore, a sample of 1,4-BDO was deposited in a xenon

Downloaded by PORTUGAL CONSORTIA MASTER on July 6, 2009
Published on April 30, 2008 on http://pubs.acs.org | doi: 10.1021/jp7116196

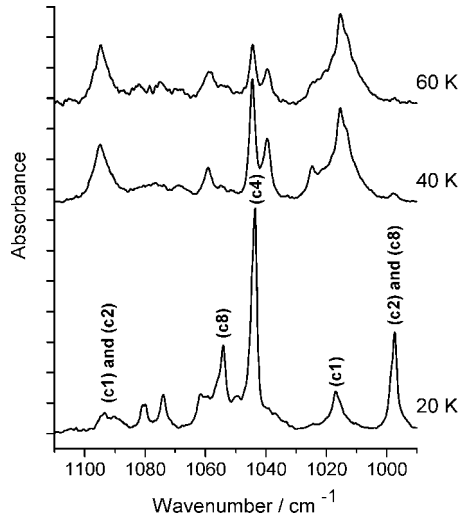

Figure 5. Infrared spectra (1110−990 cm^{-1}) of 1,4-butanediol isolated in a xenon matrix at the deposition temperature (20 K) and after annealing at 40 and 60 K.

Downloaded by PORTUGAL CONSORTIA MASTER on July 6, 2009
Published on April 30, 2008 on http://pubs.acs.org | doi: 10.1021/jp7116196

matrix at 20 K and annealed up to 60 K. Figure 5 displays the infrared spectra of 1,4-BDO isolated in that matrix at 20, 40, and 60 K. The annealing of the xenon matrix was accompanied by spectral changes indicating occurrence of conformational interconversions, with onset at 35 K, being already well-discernible at 40 K, and continuing up to higher temperatures.

In order to interpret the observed spectral changes, it should be noted once again that the conformational interconversion should occur toward the thermodynamic equilibrium, if the barriers allow so. This molecule presents, in this respect, very interesting properties. The relative values of E_0 for c1, c2, and c3 are 0, 0.45, and 1.39 kJ mol^{-1}, respectively (see Table 1), while the remaining forms have much higher energies (above 4.6 kJ mol^{-1}). This would imply that in a hypothetic thermodynamic equilibrium at 20 K these forms contribute as 93.7, 6.3, and 0.02%; at 40 K their contributions would change as 78.5, 20.3, and 1.2%; and at 60 K they would represent 68.1, 27.7, and 4.2% of the overall population, with negligible populations of other forms. Thus, the target conformational composition of the matrix after annealing would be a temperature-dependent mixture of forms c1, c2, and c3.

However, as discussed above, the target mixture should also depend on the intricate combination of possible interconversions that can be branched. On the basis of the values of the barriers to intramolecular rotation displayed in Table 6, one can assume that in the xenon matrix form c6 will be readily transformed into form c1 (barrier of 5.3 kJ mol^{-1}). Further temperature increase is expected to induce the transformations c4 → c2 (barrier of 11.6 kJ mol^{-1}) and c8 → c2 (via the c8 → c4 → c2 path). Alternatively, c8 can be transformed into c6 (barrier of 15.0 kJ mol^{-1}), which in turn is easily converted into the ground state conformer.

By the reasons described above, the experimental results of annealing are difficult to simulate theoretically, and only qualitative trends will be commented on. The most pronounced modifications involve the absorptions assigned to c1 (1092 and 1017 cm^{-1}), c2 (997 cm^{-1}), c4 (1044 cm^{-1}), and c8 (1054 cm^{-1} and tentatively 997 cm^{-1}). As expected, absorptions due to c1 steadily grew during annealing, while bands due to the less stable conformers decreased in intensity. Surprisingly, the infrared spectrum at 40 K exceeded our expectations. Besides the expected decrease of bands characteristic of forms c8 and c4, c2 was also almost depopulated in favor of c1. Due to the high energy barrier between c2 and c1 (17.2 kJ mol^{-1}), the corresponding interconversion would be expected to occur at higher temperatures, where, however, these forms should already coexist in a thermal equilibrium, so that depopulation of c2 is no longer possible. Plausible interpretations of this experimental evidence might be a slight underestimation by the MP2 calculations of the energy of c2 relative to c1 and/or an overestimation of the barrier for the c2/c1 interconversion.

3.5. Estimation of the Intramolecular Hydrogen Bond Energy. As discussed before, depending on the backbone arrangement, GG′G or G′G′G, two intramolecular hydrogen bonds of different strengths are established in 1,4-BDO. Using c1 and c2 as representative structures of these two H-bonds, their energy was estimated following three different approaches, with two of them based only on theoretical data and the other one based on the application of empirical relationships.

One of the theoretical methods used to estimate the intramolecular H-bond was based on the conformational analysis,[45,46] while the other follows a methodology recently proposed by Deshmukh et al.[47] based on the molecular tailoring approach.[48] The first one involves the direct comparison of the energy of two conformers, such that the hydrogen bond is retained in one conformer and broken in the other one and the backbone structures are not significantly changed from one another. The energy difference between the two structures is taken as the measure of an intramolecular hydrogen bond. The conformers used as reference to calculate the hydrogen bond energy of c1 and c2 were tGG′Gt (transition state structure, E_{elec} = −308.108 271 5 au) and c19, respectively. The estimated hydrogen bond energies (calculated from the electronic energy values) were found to be −19 and −13 kJ mol^{-1} for c1 and c2, respectively.

The second methodology is based on the addition and subtraction of the energies of individual fragments obtained from the original molecule (replacing an OH group by a hydrogen atom) in such a way that the energy difference between the result of addition/subtraction of the fragments and the actual energy of the conformer is due to the intramolecular hydrogen bond.[47] In the case of 1,4-BDO the fragments considered were $OHCH_2CH_2CH_2CH_3$ (F1), $CH_3CH_2CH_2CH_2OH$ (F2), and $CH_3CH_2CH_2CH_3$ (F3) and the energy of the hydrogen bond was given by

$$[E(\mathrm{F1}) + E(\mathrm{F2}) - E(\mathrm{F3})] - E(\text{optimized whole conformer})$$

Values of −23 and −17 kJ mol^{-1} were obtained for c1 and c2, respectively. The energies of the fragments are provided as Supporting Information.

Finally, the energy of the intramolecular hydrogen bond was also evaluated by the application of the empirical Iogansen equation to the spectroscopic data.[49] The values of the OH red shift ($\Delta\upsilon$) for c1 and c2 were given in the previous section. The enthalpies of the intramolecular hydrogen bond when estimated by this method were found to be −17 and −9 kJ mol^{-1} for c1 and c2, respectively.

The strengths of the intramolecular hydrogen bond in c1 estimated by the different methods here considered (−19, −23, and −17 kJ mol^{-1}) are in good agreement with each other, as well as with the value published by Mandado et al.[13] Regarding c2, for which no data were previously available in the literature, the energies of −13, −17, and −9 kJ mol^{-1} are lower than those estimated for c1. This is also consistent with what could be qualitatively expected from the NBO and AIM analyses.

4. Conclusions

In this work the structure of 1,4-BDO has been investigated by means of theoretical and experimental methods. Exploration of the entirety of the conformational space of this molecule revealed that intramolecular hydrogen bonded conformers represent about 46% of the conformational composition at 298.15 K and that the three most stable conformers are characterized by folded backbone conformations. Natural bond orbital analysis complemented by an atoms-in-molecules topological analysis enabled characterization of the main intramolecular interactions in the most abundant conformers of the molecule. In particular, the relative strengths of the intramolecular hydrogen bonding interaction in the different conformers indicate that this specific interaction is considerably stronger in the most stable conformer (c1) than in c2.

The infrared spectra of the matrix-isolated compound were found to show a good agreement with a population-weighted theoretical spectrum. The experimental spectra clearly show characteristic features of most of the conformers that are expected to be trapped in the matrixes in accordance with their calculated relative energies, interconversion barriers, and occurrence of conformational cooling during deposition of the matrixes. Annealing of the xenon matrix from 20 to 60 K resulted in significant spectral changes, which could also be successfully interpreted on the basis of the barriers to intramolecular rotation and associated conformational relaxation.

The hydrogen bond energies of c1 and c2 were estimated by means of theoretical methods and empirical correlations. For the three methodologies, the values estimated for c1 are more negative than those estimated for c2, in good agreement with the results of the relative strength of the hydrogen bond in these conformers obtained from the research methods used in this work.

Supporting Information Available: Values of the electronic energy of MP2-optimized geometries. This material is available free of charge via the Internet at http://pubs.acs.org.

References and Notes

(1) Boutron, P.; Mehl, P.; Kaufmann, A.; Angibaud, P. *Cryobiology* **1986**, *23*, 453.
(2) Mehl, P.; Boutron, P. *Cryobiology* **1987**, *24*, 355.
(3) Boutron, P. *Cryobiology* **1990**, *27*, 55.
(4) Boutron, P. *Cryobiology* **1992**, *29*, 347.
(5) Souza, E. M. T.; Teles, R. C. L.; Siqueira, E. M. A.; Freitas, S. M. *J. Protein Chem.* **2000**, *19*, 507.
(6) Romero, C. M.; Lozano, J. M.; Sancho, J.; Giraldo, G. I. *Int. J. Biol. Macromol.* **2007**, *40*, 423.
(7) Gräfje, H.; Körnig, W.; Weitz, H.-M.; Reiss, W.; Steffan, G.; Diehl, H.; Bosche, H.; Schneider, K.; Kieczka, H. Butanediols, Butenediol, and Butynediol. *Ullmann's Encyclopedia of Industrial Chemistry*, electronic release, 7th ed.; Wiley-VCH: Weinheim, 2000.
(8) Jesus, A. J. L.; Eusébio, M. E.; Redinha, J. S.; Leitão, M. L. P. *Thermochim. Acta* **2000**, *344*, 3.
(9) Jesus, A. J. L.; Rosado, M. T. S.; Leitão, M. L. P.; Redinha, J. S. *J. Phys. Chem. A* **2003**, *107*, 3891.
(10) Eusébio, M. E.; Jesus, A. J. L.; Cruz, M. S. C.; Leitão, M. L. P.; Redinha, J. S. *J. Chem. Thermodyn.* **2003**, *35*, 123.
(11) Jesus, A. J. L.; Rosado, M. T. S.; Reva, I.; Fausto, R.; Eusébio, M. E.; Redinha, J. S. *J. Phys. Chem. A* **2006**, *110*, 4169.
(12) Reva, I.; Jesus, A. J. L.; Rosado, M. T. S.; Fausto, R.; Eusébio, M. E.; Redinha, J. S. *Phys. Chem. Chem. Phys.* **2006**, *8*, 5339.
(13) Mandado, M.; Mosquera, R. A.; Van Alsenoy, C. *Tetrahedron* **2006**, *62*, 4243.
(14) Howard, D. L.; Kjaergaard, H. G. *J. Phys. Chem. A* **2006**, *110*, 10245.
(15) Klein, R. A. *J. Comput. Chem.* **2003**, *24*, 1120.
(16) Fishman, E.; Chen, T. L. *Spectrochim. Acta, Part A* **1969**, *25*, 1231.
(17) Foster, A. B.; Haines, A. H.; Stacey, M. *Tetrahedron* **1961**, *16*, 177.
(18) Kuhn, L. P. *J. Am. Chem. Soc.* **1952**, *74*, 2492.
(19) Shagidullin, R. R.; Chernova, A. V.; Shagidullin, R. R. *Russ. Chem. Bull.* **1993**, *42*, 1505.
(20) Traetteberg, M.; Hedberg, K. *J. Am. Chem. Soc.* **1994**, *116*, 1382.
(21) Frisch, M. J.; Head-Gordon, M.; Pople, J. A. *Chem. Phys. Lett.* **1990**, *166*, 281.
(22) Frisch, M. J.; Head-Gordon, M.; Pople, J. A. *Chem. Phys. Lett.* **1990**, *166*, 275.
(23) Head-Gordon, M.; Head-Gordon, T. *Chem. Phys. Lett.* **1994**, *220*, 122.
(24) Peng, C. Y.; Ayala, P. Y.; Schlegel, H. B.; Frisch, M. J. *J. Comput. Chem.* **1996**, *17*, 49.
(25) Frisch, M. J.; Trucks, G. W.; Schlegel, H. B.; Scuseria, G. E.; Robb, M. A.; Cheeseman, J. R.; Montgomery, J. A., Jr; Vreven, T.; Kudin, K. N.; Burant, J. C.; Millam, J. M.; Iyengar, S. S.; Tomasi, J.; Barone, V.; Mennucci, B.; Cossi, M.; Scalmani, G.; Rega, N.; Petersson, G. A.; Nakatsuji, H.; Hada, M.; Ehara, M.; Toyota, K.; Fukuda, R.; Hasegawa, J.; Ishida, M.; Nakajima, T.; Honda, Y.; Kitao, O.; Nakai, H.; Klene, M.; Li, X.; Knox, J. E.; Hratchian, H. P.; Cross, J. B.; Bakken, V.; Adamo, C.; Jaramillo, J.; Gomperts, R.; Stratmann, R. E.; Yazyev, O.; Austin, A. J.; Cammi, R.; Pomelli, C.; Ochterski, J. W.; Ayala, P. Y.; Morokuma, K.; Voth, G. A.; Salvador, P.; Dannenberg, J. J.; Zakrzewski, V. G.; Dapprich, S.; Daniels, A. D.; Strain, M. C.; Farkas, O.; Malick, D. K.; Rabuck, A. D.; Raghavachari, K.; Foresman, J. B.; Ortiz, J. V.; Cui, Q.; Baboul, A. G.; Clifford, S.; Cioslowski, J.; Stefanov, B. B.; Liu, G.; Liashenko, A.; Piskorz, P.; Komaromi, I.; Martin, R. L.; Fox, D. J.; Keith, T.; Al-Laham, M. A.; Peng, C. Y.; Nanayakkara, A.; Challacombe, M.; Gill, P. M. W.; Johnson, B.; Chen, W.; Wong, M. W.; Gonzalez, C.; Pople, J. A. *Gaussian 03*, revision D.01; Gaussian, Inc.: Wallingford, CT.
(26) Glendening, E. D.; Badenhoop, J. K.; Reed, A. E.; Carpenter, J. E.; Bohmann, J. A.; Morales, C. M.; Weinhold, F. *NBO 5.G*; Theoretical Chemistry Institute, University of Wisconsin: Madison, http://www.chem.wisc.edu/nbo5.
(27) Schmidt, M. W.; Baldridge, K. K.; Boatz, J. A.; Elbert, S. T.; Gordon, M. S.; Jensen, J. H.; Koseki, S.; Matsunaga, N.; Nguyen, K. A.; Su, S.; Windus, T. L.; Dupuis, M.; Montgomery, J. A. *J. Comput. Chem.* **1993**, *14*, 1347.
(28) Bader, R. F. W. *Atoms in Molecules—A Quantum Theory*; University Press: Oxford, 1990.
(29) Biegler-König, F. W.; Bader, R. F. W.; Tang, W.-H. *J. Comput. Chem.* **1982**, *3*, 317.
(30) Bader, R. F. W. *AIMPAC, Suite of programs for the Theory of Atoms in Molecules*; McMaster University: Hamilton, Ontario, Canada.
(31) Steiner, T. *Angew. Chem., Int. Ed.* **2002**, *41*, 48.
(32) Jeffrey, G. A. *An Introduction to Hydrogen Bonding*; Oxford University Press: Oxford, 2002.
(33) Weinhold, F.; Landis, C. R. *Valency and bonding: A Natural Bond Orbital Donor-Acceptor Perspective*; Cambridge University Press: New York, 2005.
(34) Weinhold, F.; Landis, C. R. *Chem. Educ. Res. Pract.* **2001**, *2*, 91.
(35) Reed, A. E.; Curtiss, L. A.; Weinhold, F. *Chem. Rev.* **1988**, *88*, 899.
(36) Foster, J. P.; Weinhold, F. *J. Am. Chem. Soc.* **1980**, *102*, 7211.
(37) Weinhold, F. *NBO 5.0 Program Manual*; Theoretical Chemistry Institute, University of Wisconsin: Madison, 2001.
(38) Weinhold, F. *THEOCHEM* **1997**, *398–399*, 181.
(39) Koch, U.; Popelier, P. L. A. *J. Phys. Chem.* **1995**, *99*, 9747.
(40) Pacios, L. F.; Gómez, P. C. *J. Comput. Chem.* **2001**, *22*, 702.
(41) Klein, R. A. *Chem. Phys. Lett.* **2006**, *425*, 128–133.
(42) Barnes, A. J. *J. Mol. Struct.* **1984**, *113*, 161.
(43) Felder, P.; Gunthard, H. H. *Chem. Phys.* **1982**, *71*, 9.
(44) Reva, I. D.; Stepanian, S. G.; Adamowicz, L.; Fausto, R. *Chem. Phys. Lett.* **2003**, *374*, 631.
(45) Estácio, S. G.; Couto, P. C.; Cabral, B. J. C.; Minas da Piedade, M. E.; Martinho Simões, J. A. *J. Phys. Chem. A* **2004**, *108*, 10834.
(46) Korth, H. G.; de Heer, M. I.; Mulder, P. *J. Phys. Chem. A* **2002**, *106*, 8779.
(47) Deshmukh, M. M.; Gadre, S. R.; Bartolotti, L. J. *J. Phys. Chem. A* **2006**, *110*, 12519.
(48) Ganesh, V.; Dongare, R. K.; Balanarayan, P.; Gadre, S. R. *J. Chem. Phys.* **2006**, *125*, 104109.
(49) Iogansen, A. V. *Spectrochim. Acta, Part A* **1999**, *55*, 1585.

JP7116196

Downloaded by PORTUGAL CONSORTIA MASTER on July 6, 2009
Published on April 30, 2008 on http://pubs.acs.org | doi: 10.1021/jp7116196